8-2004

Analytical and Computational Model for Aortic Hemodynamics Accounting for Aortic Elasticity and Arterial Branch-Flow Effects

Amber Adriann Hensley Edwards
University of Tennessee - Knoxville

To the Graduate Council:

I am submitting herewith a thesis written by Amber Adriann Hensley Edwards entitled "Analytical and Computational Model for Aortic Hemodynamics Accounting for Aortic Elasticity and Arterial Branch-Flow Effects." I have examined the final electronic copy of this thesis for form and content and recommend that it be accepted in partial fulfillment of the requirements for the degree of Master of Science, with a major in Mechanical Engineering.

Joe Iannelli, Major Professor

We have read this thesis and recommend its acceptance:

Richard J. Jendrucko, David J. Keffer

Accepted for the Council:
Dixie L. Thompson

Vice Provost and Dean of the Graduate School

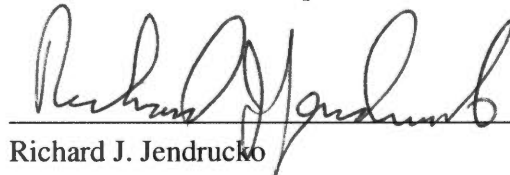(Original signatures are on file with official student records.)
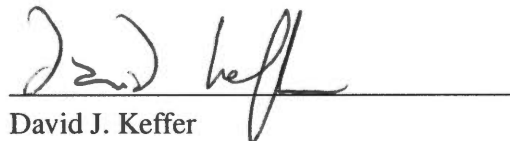
To the Graduate Council:

I am submitting herewith a thesis written by Amber Adriann Hensley Edwards entitled "Analytical and Computational Model for Aortic Hemodynamics Accounting for Aortic Elasticity and Arterial Branch-Flow Effects". I have examined the final paper copy of this thesis for form and content and recommend that it be accepted in partial fulfillment of the requirements for the degree of Master of Science, with a major in Mechanical Engineering.
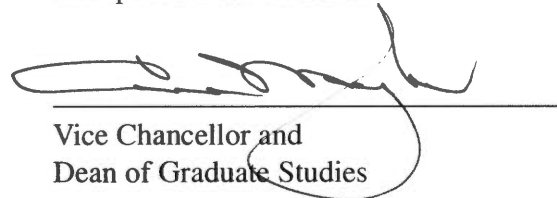
Joe Iannelli, Major Professor

We have read this thesis
and recommend its acceptance:

Richard J. Jendrucko

David J. Keffer

Accepted for the Council:

Vice Chancellor and
Dean of Graduate Studies

Analytical and Computational Model for Aortic Hemodynamics Accounting for Aortic Elasticity and Arterial Branch-Flow Effects

A Thesis
Presented for
Master of Science Degree
The University of Tennessee, Knoxville

Amber Adriann Hensley Edwards

August 2004

Dedication

This thesis is dedicated to my very supportive and loving husband Dean Edwards - I Love You, to my wonderful parents, Noble and Fran Hensley, who taught me to put God first and gave me wind for my wings that allowed me to fly higher than I ever could have by myself, to my wonderful brother Anthony Hensley to whom I admire and look up to, to my Uncle George and Aunt Bonnie whose prayers and encouragement over these past seven years has meant so much to me, to the great friends God has blessed me with, and to my mentor and major professor Dr. Joe Iannelli. This thesis is also dedicated to all those who have suffered from anxiety and panic disorder -

> Far better it is to dare mighty things, to win glorious triumphs, even though checked by failure, than to rank with those poor spirits who neither enjoy much nor suffer much, because they live in the grey twilight that knows neither victory or defeat. – Theodore Roosevelt

Acknowledgements

I would not have made it this far without the support, love, and prayers of so many wonderful people. As I look back over the past seven years that I have been in college, I think about how thankful I am to my Lord Jesus Christ for everything I have been able to accomplish. This road I have traveled has had many ups and downs. I've found myself on my knees many times praying for direction and just needing someone to complain to. He always listened and never failed to comfort me. He has also brought into my life a wonderful person, my husband Kevin Dean Edwards, who has helped me laugh through the tears and forced me to go outside and smell the roses. I would like to thank him for the relaxing late-night walks outside while I was writing this thesis, even if all I did was watch him take pictures of moths and listen to owls. Dean, I love your gentle nature and the way that you love me. You have brought so much joy to my life. Thanks for always loving me unconditionally and for dreaming my dreams with me. I could not have done this without your love and encouragement. I love you so very much. Oh, yes, and thanks for all the Silly Putty you have bought me to add to my collection. You always know how to brighten my days.

I want to thank my Mom and Dad, Fran and Noble Hensley, for their love and support as well. I started out wanting to be a physician and here I am, an engineer. Thanks for letting me find my own way and for supporting my decisions. You always knew when to hold on and when to let go. I have had to sacrifice many things to get this degree. There

were times when I wanted to go to dinner or just come over to the house and spend time with you but could not due to my work. I look forward to making up for lost time spent apart, to being there on birthdays and eating lunch with you on Sundays instead of rushing home to do homework or study for tests. Thanks for allowing me to follow after my dreams even if they did take me several miles away one summer to George Washington University. I know you burned the midnight oil many times praying for me, especially during times when I was discouraged and needed answers. Thanks, he listened and always came through. You are simply the best parents any one could ever dream about, let alone have – I love you!

I would like to also thank my brother, Anthony, for his encouragement. I am so proud of everything that he has accomplished as a mining and mineral engineer. You always understood what I was going through in engineering and were so supportive. You are not only a brother to me, but a friend. Even though we have been several hours apart for the past few years, you have only been a phone call away and you always took the time to listen. I look forward to Dean and me spending more time with you and Tinsley. I love you very much and am so proud of you and the person you are. I admire the way you reach out to others and give so much of yourself to help those in need.

I would like to thank my mentor and major professor, Dr. Joe Iannelli. Thanks for giving me this wonderful project to work on and for believing in me. Thanks for all the support you have given me throughout my six years at the University of Tennessee, Knoxville and for helping me reach my goals and achieve my dreams. Whenever I needed a tutor, your office light was always on. You have always put the student before yourself and because of that you have made such a positive impact on so many lives, including mine. Thanks for helping me believe in myself and gain self-confidence.

I would also like to give a special thanks to my hound dogs, Winnie and Eeyore. What would I do if I did not have you in my life. Dean let me bring Winnie home from the shelter

a few months ago when I was going through a difficult time. Winnie has brightened my days and the sadness I felt inside began to disappear with every lick in the face and wag of the tail. Over the past few months, we have been inseparable. She is truly a gift from God. Eeyore, has seen both Dean and I through several years of school and I think he is excited to see us both getting done. Thanks, Eeyore, for being so understanding when we could not take long walks at night or swims in the lake because there was just to much work to do. We definitely need to buy you a big bone and take you to the park.

Abstract

The causes of atherosclerotic plaque formation in the abdominal aorta has been researched for many years. It has been hypothesized that certain hemodynamic factors, such as wall shear stress, blood velocity, and blood pressure, may play an important role in its development. In order to study these properties, several models have previously been developed to try and simulate blood flow through the abdominal section of the aorta since it is at this location along the length of the aorta where the greatest incidence of atherosclerosis is known to occur. Many of these models depict the abdominal aorta as being a rigid tube and do not account for elasticity. In this study an analytical and computational model that accounts for both elasticity and taper is developed. This model is used to determine the effects that blood flow through the abdominal aorta, when modeled as a straight rigid tube, straight elastic tube, tapered rigid tube, and tapered elastic tube without branches, has on the blood velocity, blood pressure, wall shear stress, and anatomical and physiological diameters. The effect that the seven major branch flows has on these hemodynamic factors is also studied. It has been found that taper and elasticity do have an effect and certainly should be accounted for when modeling the aorta. It has also been found that the addition of branch flows causes the blood velocity and wall shear stress to decrease at the infrarenal section of the abdominal aorta. Other studies have found that it is at this location along the aorta where atherosclerotic plaque is more prone to develop.

Contents

List of Tables

List of Figures

Chapter 1

Background

1.1 Arterial Wall-Structure of the Aorta

The large arteries, such as the aorta and its major branches, are known as elastic arteries. A discussion on the structure of the arterial wall assists in understanding the difficulty in establishing the mechanical properties of the wall and the use of an average modulus of elasticity for the wall. As shown in **Figure 1.1**, there are three distinct layers that form the aorta's artery wall: the tunica intima (innermost layer), tunica media (middle layer), and tunica externa or adventitia (outermost layer) (Spence and Mason 1987).

The tunica intima is the section of the artery that extends from the luminal endothelial lining to the internal elastic lamina. The intima consists of three layers. The first layer is simple squamus epithelium known as endothelium. This endothelial cell layer is composed of a continuous monolayer of flat, elongated, polygonal cells aligned in the direction of blood flow and, unlike the other layers, is the immediate interface between the bloodstream and the underlying arterial wall and plays a very important role in the formation of atherosclerotic plaques. Both normal forces due to blood pressure and drag forces due to blood flow act on this layer. Experimental evidence has shown that this layer

1
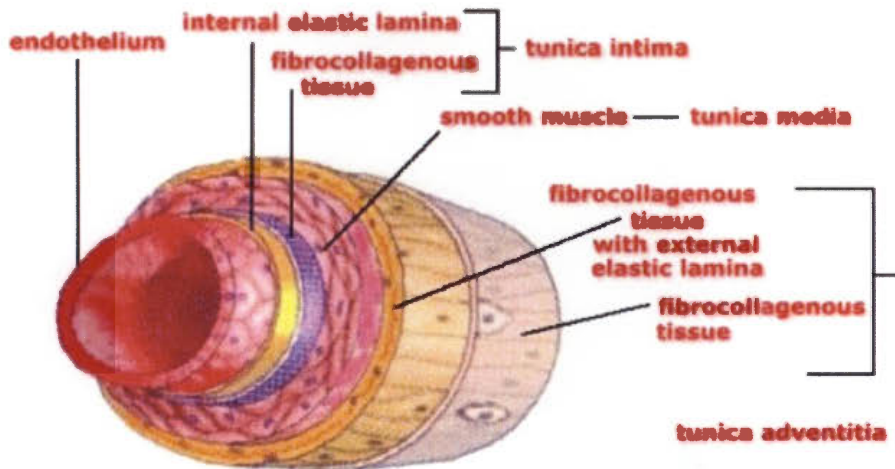
Figure 1.1: *Structure of artery (Ross 1999).*

can withstand high shear stresses and acts as a thrombosis-resistant surface as well as a selective interface for convection, diffusion, and active transport of circulating substances into the underlying arterial wall; therefore, it plays an important role in the movement of lipoproteins and other agents that can lead to the build-up of atherosclerotic plaques in the artery. The second intima layer is composed of connective tissue, and the third layer is a basement membrane commonly known as the basal lamina which provides a junction that allows for the bending or changing of the diameter or configuration of the artery most associated with pulse pressure which in turn prevents the disruption or detachment of endothelium. The tight rigid junctions may also help prevent telescoping imposed by shear stresses due to blood flow (Wilson *et al.* 1987).

The tunica media is defined as the section that extends from the internal elastic lamina to the adventitia. The media is thick and is composed of closely packed layers of smooth muscle cells (circularly arranged) mixed with elastin and collagen fibers. The elastic fibers are extensible and allow for a certain degree of compliance. The fibers recoil during the cardiac cycle and distribute mural tensile stresses uniformly. The collagen fibers provide

2

tensile strength to the media and have a high modulus of elasticity that prevents disruption (Wilson *et al.* 1987).

The adventitia is a thin layer of connective tissue that consists of both elastic and collagenous fibers that run parallel to the artery axis. This layer aides in holding vessels open and keeps vessels from tearing during movement of the body (Thibodeau and Patton 1996). The adventitia of the muscular arteries and major elastic arteries, such as the aorta, contains vasa vasorum and venous channels that give nutrition to the artery wall. In some instances where an intimal atherosclerotic plaque is present on an atrophic media, a thickened adventitia may play an important role in giving structural support to the artery wall. (Wilson *et al.* 1987). This multi-layer structure leads to an average modulus of elasticity for the wall of $E = 4.4e^5$ Pa (Bergel 1961).

Arteries, in general, increase in diameter, elongate, and become twisted with age. The enlargement of an artery, such as the aorta, is known as ectasia. When ectasia occurs in the aorta, there tends to be an increase in both the matrix fiber accumulation and the collagen content, calcification of the elastic fibers, and a decrease in both its elastin content and wall compliance. However, due to these changes, certain complications can occur which can lead to the formation of atherosclerosis (Wilson *et al.* 1987).

1.2 Atherosclerosis

1.2.1 Atherosclerotic Lesion Structure

Atherosclerosis is a common type of vascular disease that most often develops in the aorta. This disease alters the shape of the vessel and can, therefore, severely affect the blood flow and associated distributions of pressure and wall shear stress as shown in **Figure 1.2**. Atherosclerosis has been identified in humans for thousands of years; for instance, lesions

3
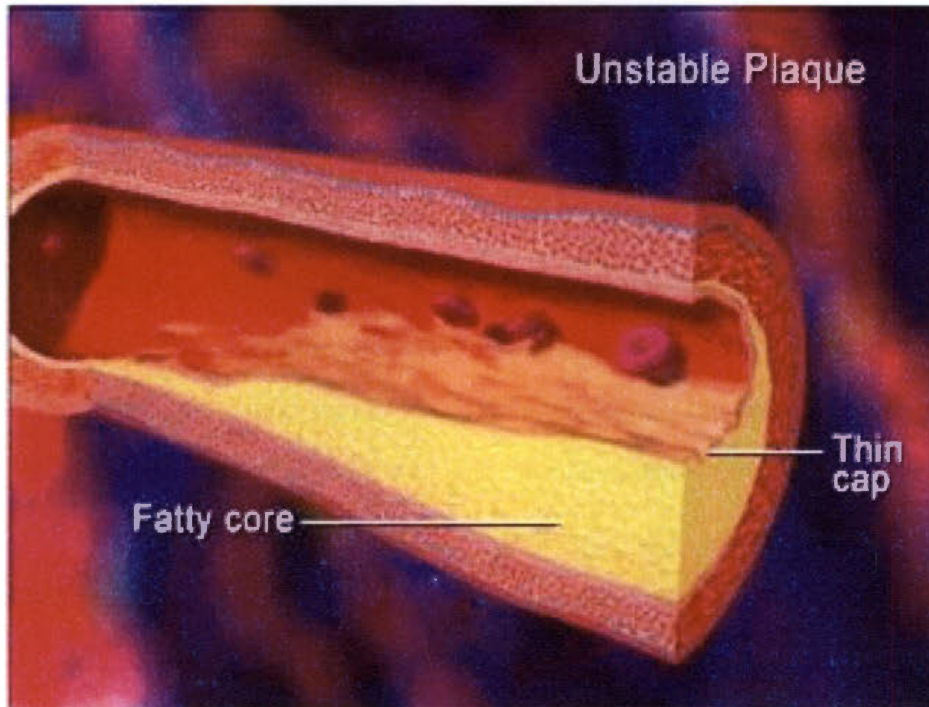
Figure 1.2: *Schematic of Atherosclerotic Plaque Build-up in Artery.*

have been found in Egyptian mummies dating back to the fifteenth century B.C. It has been found that the atherosclerotic lesions can take different forms depending upon their anatomical location; the age, genetic and physiological status of the affected individual; and whether or not the individual has been exposed to certain risk factors such as diabetes mellitus, high-fat and high-cholesterol diets, hypertension, and smoking. The lesions, of which there are three types, often occur in the intima. They include the fatty streak, the fibrous plaque, and the so-called complicated lesion (Wilson *et al.* 1987).

Fatty streaks may appear as yellow patches on the luminal surface of an individuals' aorta soon after birth and are observed to be on most aortas of individuals over the age of three; however, they are found more frequently in individuals that are 8-18 years of age. The fatty streaks are composed of both lipid-laden macrophages and smooth-muscle cells,

which contain cholesterol and cholesterol oleate deposits; however, they do not appear to cause any arterial obstruction. The fatty steaks are found to be present in young people and in populations that never appear to develop atherosclerosis. This finding has lead scientists to believe that, since some fatty streaks found in individuals resolve, certain events must occur in the fatty streaks of other individuals that lead to the development of fibrous plaque, a more complex atherosclerotic formation (Wilson *et al.* 1987).

The fibrous plaque usually starts to develop at 25 years of age in populations in which the incidence of atherosclerosis is high. The plaque becomes elevated and can extrude through the lumen of the artery. If it continues to progress, it can jeopardize the vascular supply of the tissue involved and block the lumen. Also, during the formation of the fibrous plaque, smooth-muscle cells proliferate within the arterial intima. The cell proliferation process creates a fibrous cap which covers a deep core consisting of new connective tissue cell and intracellular and extracelluar lipid deposits. It is believed, but not proven, that fatty streaks that continue the process of cell proliferation, connective tissue formation, and lipid formation create the fibrous plaque. If the fibrous plaque becomes vascularized, complicated lesions may form (Wilson *et al.* 1987).

The complicated lesions occur as the patient's age increases. The lipid core becomes calcified and increases in size and the fibrous cap becomes very thin. It may also be interrupted or disrupted focally which causes the underlying lesion contents to enter the bloodstream forming thrombi. The thrombi may then organize and increase the plaque thickness while decreasing the arterial lumen size which can obstruct the blood flow. As the lesion continues to grow in the intima layer of the artery, the number of smooth-muscle cells in the media decrease and cause the media to deteriorate which can result in changes that may lead to an aneurysm (Wilson *et al.* 1987).

1.2.2 Location of Atherosclerotic Plaques

Aortic atherosclerotic plaques are often found in the descending thoracic section of the adult human aorta. However, they are usually not as abundant and are less complicated than the plaques found in the infrarenal abdominal aorta. The reason why plaques are more prone to form in the abdominal aorta than in the thoracic is believed to be due to the difference in blood flow velocity. For instance, the velocity of blood flow through the thoracic aorta is high since it is the major conduit for the constant elevated levels of flow to the cerebral, upper extremity, and visceral arterial beds (Wilson *et al*. 1987). The thoracic aorta also delivers one-quarter of the cardiac output to the renal arteries. In contrast, the velocity of blood flow through the abdominal aorta is mainly dependent on muscular activity in the lower extremities. Over long term, the abdominal aorta's blood flow often decreases due to an increasing inactive lifestyle and to the normal tendency of the aorta to increase in diameter with increasing age. There is also a difference in the media of the thoracic aorta as opposed to that of the abdominal aorta. The media of the thoracic contains intramural vasa vasorum while the abdominal aorta is mainly avascular (Wilson *et al*. 1987). These differences in combination are believed to increase the formation of atherosclerotic plaque in the abdominal aorta, which accounts for 15% of the total cases of atherosclerosis reports and 6% of atherosclerosis related deaths (anon. 1981).

1.3   Previous Studies of Hemodynamic Factors

The patchy distribution of atherosclerotic lesions with predilection sites at branches and arterial curvatures in the arteries has led researchers to believe that there may be a direct correlation between local hemodynamics and the development of atherosclerosis (Pedersen *et al*. 1999). The main local hemodynamic factor for initiating atherosclerotic plaques is believed, by some researchers, to be the wall shear stress, which is the dynamic inter-

6

action between the flowing blood and the vessel wall (Pedersen *et al.* 1993). Research has shown that the wall shear stress plays an important role in the initial endothelial injury that precedes the chronic inflammatory response of atherosclerosis in both endothelial cell cultures and genetically modified animal models. It has also been shown that one of the first steps in the atherosclerotic process is the sensing of low and/or oscillating wall shear stress by endothelial cells. This causes the endothelial cells to upregulate their expression of cellular adhesion molecules at certain sites. These upregulation sites have been found to be the location of atherosclerotic lesions (Pedersen *et al.* 1999).

Pedersen *et al.* (1999) found that wall shear stresses measured *in vitro* in young adult autopsies correlate with the location of early atherosclerotic lesions. They also studied whether this correlation would hold true when measuring wall shear stresses *in vivo* by magnetic resonance. In this study wall shear stress was measured in six volunteers who did not have a history of cardiovascular disease. Their ages ranged from 23-30. Measurements were taken 1.5 cm above the coeliac trunk and 3.5 cm above the abdominal aortic bifurcation. The wall shear stress was found at the anterior, posterior, left and right vessel walls at the suprarenal and infrarenal positions. Also, ten aortas were obtained by autopsy in order to measure the thickness of the intima, which was done at the same axial suprarenal and infrarenal positions. It was found that the maximum and mean wall shear stresses were at their highest at the suprarenal location and at their lowest at the infrarenal location where the oscillating shear index was at its highest. Differences in the magnitude of the wall-shear measurements in the infrarenal aorta were seen between the anterior and posterior vessel wall. The highest mean and maximum wall shear stresses were found at the anterior vessel wall whereas the minimum wall shear stresses were found at the posterior vessel wall where the oscillating shear index was also at its highest. It was also found that the intima thickness showed a linear decrease with the mean wall shear stress and a linear increase with the oscillating shear index. Therefore, Pedersen *et al.* (1999)

concluded that the data obtained did agree with the previous hypothesis based on indirect *in vivo*, *in vitro*, or animal studies that found low or oscillating wall shear stresses are a localizing factor for intimal thickening and favor the formation of atherosclerosis.

Although the wall shear stress is believed by many to be the main hemodynamic factor in initiating the development of atherosclerosis, it is speculated that other hemodynamic factors, such as cyclic strain and pressure forces may play an important role as well. Glagov *et al.* (1988) speculated that turbulence and disturbed flows cause atherosclerosis. Fox and Hugh (1966) suggested that blood flow pattern variations, specifically boundary-layer separation, could also play a significant part in the formation of atherosclerosis.

Research has shown that hemodynamic conditions change in the abdominal aorta according to differing physiological needs. For instance, under normal resting conditions, measurements by Sapirstein indicate that two-thirds of the blood from the thoracic aorta flows to the arteries that branch off the aorta at the diaphragm (Sapirstein 1958). Under heavy exercise conditions such as running or bicycling, the blood flow through the aorta increases by over eight times that of normal resting blood flow. Most of this increase goes to supply the lower limbs. This increase in blood flow to the limbs may be as high as 800%. Because of this increased need for blood in the legs and the constant blood supply to the abdominal organs, the percentage of thoracic aorta blood flow exiting the four vessels at the diaphragm decreases from 65% to about 20% (Moore and Ku 1994b). The volumetric blood flow rates obtained by Sapirstein through the abdominal aorta under resting and exercise conditions are shown in **Table 1.1**.

These changes in hemodynamic conditions that occur under different physiological conditions are indeed very significant. In fact, there is evidence that clinical incidence and symptoms of atherosclerosis may be abated by exercise. This may be attributed to the fact that chronic increases in blood flow, which occurs under exercise conditions, stimulate the expression of both nitric oxide synthase and superoxide dismutase. These chemicals

8

Table 1.1: *Blood flow rates (L/min) in the human abdominal aorta under resting and exercise conditions (Sapirstein 1958).*

Artery	Rest	Exercise
Celiac	0.59	0.29
Superior Mesenteric	0.40	0.23
Left Renal	0.40	0.29
Right Renal	0.40	0.29
Inferior Mesenteric	0.13	0.05
Left Iliac	0.40	2.68
Right Iliac	0.40	2.68

reduce the concentration of cellular superoxide anion (O_2^-), the expression of monocyte chemotactic protein-1, and vascular cell adhesion molecule-1 (Cybulsky and Gimbrone 1991; Nobutaka *et al.* 1996). It has been hypothesized that these effects may reduce the endothelial adhesiveness of monocytes and protect the vascular endothelium from atherosclerotic plaques. The elevated shear stress which would occur with the increase in blood flow also causes cells to elongate in the direction of maximum stress. This elongation is also believed to inhibit the formation of atherosclerosis (Zarins *et al.* 1981). Because of these findings, there has been a great deal of research devoted to determining the physiological changes that occur under rest and exercise conditions.

Wang *et al.* found that even short periods of exercise in a canine enhances acetylcholine-induced dilation of the large coronary artery and hypothesized that the enhancement can be contributed to increased levels of endothelium relaxation factor, nitric oxide (EDRF/NO). Also, it is hypothesized that the coronary dilation and the increased release of EDRF/NO is due to the upregulation of NO in the coronary vascular endothelial cells (Wang *et al.* 1993). Furthermore, Sessa *et al.* found that chronic exercise in canines causes the nitric oxide synthase gene to be expressed (Sessa *et al.* 1994). The expression of this gene along

9

with the other added benefits of exercise, which include enhanced cholesterol metabolism, lower blood pressure, and increased blood flow and wall shear stress, may all be important contributing factors to one's cardiovascular health (Taylor *et al.* 2002).

Taylor *et al.* studied the spatial distribution of blood flow velocities, *in vivo*, in the abdominal aorta of humans during upright rest and light exercise conditions. Six 20–24-year-old healthy males and five 23–28-year-old healthy females were chosen to be imaged during rest and exercise. Subjects close to the same age were chosen due to the findings of Strong *et al.* (1999) which stated that less than 4% of a representative population with the same age profile experience hemodynamically significant atherosclerotic lesions. The subjects were seated on a custom MR-compatible bicycle in a 0.5-T open magnet. Subjects were scanned at rest and steady-state exercise conditions. Cine-phase contrast MRI techniques were implemented to measure the blood flow velocity as a function of position at the supraceliac, suprarenal, and infrarenal levels under conditions of both rest and exercise. Spatial maps of magnitude and velocity that described the anatomy and blood flow were obtained at each of the three aorta levels. Heart rates in the subjects increased from 73 ± 6.2 beats/min at rest to 110 ± 8.8 beats/min during exercise. Taylor *et al.* found that significant changes in blood flow through the abdominal aorta was a result of the heart rate change and increased metabolic demand in the lower limbs during exercise. Under conditions of rest, the flow rate in the supraceliac was positive throughout the cardiac cycle and did not reach zero during early diastole. A period of reverse flow was observed in the infrarenal aorta in early diastole and the volumetric flow rate was found to be close to zero for the remainder of diastole. The velocity data obtained showed that blood flow reversal occurs near the lumen boundary. Under conditions of exercise, there was a significant increase in the volumetric flow rate, which remained positive throughout the cardiac cycle, at the supraceliac and infrarenal levels (Taylor *et al.* 2002).

The total blood flow through the abdominal aorta increased from 2.9 ± 0.6 L/min at

10

rest to 7.2 ± 1.4 L/min under exercise conditions; the blood flow to the digestive and renal circulations decreased from 2.1 ± 0.5 L/min at rest to 1.6 ± 0.7 L/min during exercise; and the blood flow to the infrarenal aorta increased from 0.9 ± 0.4 L/min at rest to 5.6 ± 1.1 L/min during exercise. Blood flow reversal was observed in the infrarenal aorta only under conditions of rest. It was also found that the mean wall shear stress increased from 3.5 ± 0.8 dyn/cm^2 at rest to 6.2 ± 0.5 dyn/cm^2 during exercise in the supraceliac aorta and the oscillatory shear index (OSI) at this level was 0 in both rest and exercise conditions. These values increased from 1.3 ± 0.6 dyn/cm^2 at rest to 5.2 ± 1.3 dyn/cm^2 during exercise in the infrarenal aorta and the OSI decreased from 0.1 ± 0.1 at rest to 0 during exercise (Taylor *et al.* 2002).

As a result of this study, Taylor *et al.* found that the reduction in flow oscillations, increased wall shear stresses, and reduced shear stress oscillations that occur in the infrarenal aorta are all measured effects of exercise. This supports the idea that exercise provides local benefit in vasculature portions by eliminating hemodynamic conditions that are believed to correlate with atherosclerotic plaque locations (Taylor *et al.* 2002).

Moore and Ku studied the changes in the blood velocity vector profiles in the abdominal aorta that would be expected to occur under exercise conditions. They also compared the physiological changes that take place under exercise conditions to those occurring at a state of rest. In order to do so, a glass-blown model of the aorta was used, in which water was used to simulate blood flow. The model had dimensions based on the average measurements of ten cadaver aortas and fifty-five bi-planar angiograms and constituted seven major branches: the celiac artery, the superior mesenteric artery, the right and left renal arteries, the inferior mesenteric artery, and the right and left common iliac arteries. The thoracic aorta mean flow rate for exercise conditions increased by 240% over the resting value. The percentage of blood that flowed to the iliac arteries from the thoracic aorta increased from 30% to 80% which resulted in an iliac blood flow increase of 670%. The

11

pulse rate was 130 beats/min for exercise conditions as opposed to 70 beats/min for resting conditions (Moore and Ku 1994b).

Moore and Ku found that the hemodynamic flow in an aortic model under differing physiological conditions showed significant changes from the resting state. Under exercise conditions, the flow in the aorta was forward and undisturbed throughout the cardiac cycle. The flow reversal in the abdominal aorta in the exercise case was less than one-fourth of that seen in the resting case, and the velocity profiles were more symmetric. The flow reversal was less than that found at a state of rest due to the increase in the flow rate that occurs under exercise conditions. The velocity measured in the suprarenal aorta was found to be more than 50 cm/s, which is approximately two-times greater than the resting value. There was a decrease in flow reversal in the aortic bifurcation and the infrarenal aorta under exercise conditions than. The increase in velocity and the decrease in the flow reversal that Moore and Ku found under the exercise conditions are believed to reduce the rate of the progression of atherosclerosis and affect the symptoms from occlusive atherosclerosis (Moore and Ku 1994b).

Pedersen *et al.* (1993) also conducted a study to try to obtain two-dimensional quantitative velocity data from an anatomically and physiologically realistic flow model of the abdominal aorta taking special interest in determining what influence (if any) the differing flow conditions that occur during rest and exercise have on this area of the vascular tree. Pedersen *et al.* (1993) also wanted to annotate, in greater detail, the relationship that exists between the localization of the atherosclerotic lesions and the local hemodynamics. In order to do this study, a 22-year-old human male cadaver abdominal aorta was harvested. The diameters of the vessels, the branch angles, and the aortic-arch curvature were measured. From these measurements, a glass model, similar to the one Moore and Ku (1994b) developed, was blown. The branch vessels included in the model were the celiac trunk, superior mesenteric artery, renal arteries, and the common external and inter-

12

nal iliac arteries. The flow rates in the branches were also based on the values that Moore and Ku used in their study. The model used was mounted in a pulsatile flow loop. In order to simulate the pressure and physiologic flow conditions that occur in the abdominal aorta at rest, during medium exercise and exercise, the loop was built-up as a left heart and aorta simulator. The flow of blood, which was an aqueous solution of glycerin having a kinematic viscosity of 3.3×10^{-6} m^2/s, was regulated by precision valves before entering a system that had a constant outflow pressure of 50 mm of Hg to the branches (Pedersen *et al.* 1993).

Pedersen *et al.* (1993) found that, under resting conditions, the suprarenal abdominal aorta (SAA) velocity profiles were flat and symmetric. The flow direction in the center of the aorta was found to be antegrade (or normal) and small retrograde velocities were seen at the vessel walls during early diastole. At the proximal infrarenal abdominal (PIAA) position, the velocity profiles were skewed and the highest velocities were present at the anterior vessel wall. During early diastole, retrograde flow was also present across the entire aorta diameter. At the distal infrarenal abdominal aorta position, the axial velocity profiles were slightly skewed during systole and were more evident during early diastole during which the highest retrograde velocities were at the posterior vessel wall. A zone of retrograde velocities were also visible later in diastole in the posterior half of the vessel, and vessel velocities in the anterior half were antegrade. Also, under conditions of rest, the oscillating shear index showed oscillating wall shear stresses for all the infrarenal positions were large and were very small for the suprarenal positions (Pedersen *et al.* 1993).

Under exercise conditions the velocity profiles were flat and symmetric at the SAA position as they were in the resting condition. Minimum velocities near the aortic wall had antegrade direction and no retrograde velocities were observed unlike the small retrograde velocities that were visible under resting conditions. Unlike the resting condition, there was no skewing of the profiles present at the PIAA position. However, in systole, coher-

13

ent structures were visible in the anterior part of the vessel and, in diastole, retrograde velocities were seen at the posterior vessel walls and at the anterior walls. At the DIAA position, velocity profiles were more prominent and had a slight skewness towards the anterior wall. The oscillating wall shear stresses under exercise conditions were mostly present at the posterior vessel wall in the distal infrarenal position (Pedersen *et al.* 1993).

The study by Pedersen *et al.* (1993) found that there are major differences in the localization of the low and non-oscillating shear stresses between the suprarenal and infrarenal abdominal aorta. Pedersen *et al.* also found that the low-velocity and oscillating shear stress regions found in the study correlated with previously published data on the distribution of atherosclerotic lesions. In one of these previous studies (Cornhill *et al.* 1990), it was observed that atherosclerotic lesions were more prone to develop at the posterior vessel wall in the infrarenal abdominal aorta, especially in the distal part, and at the anterior vessel wall located between the right renal and left renal arteries and the inferior mesenteric artery. These locations did, in fact, correspond with the locations found in the Pedersen *et al.* study at which the velocity was low and the oscillating shear stress was present (Pedersen *et al.* 1993).

Chapter 2

Problem Statement

Previous studies on the aorta, including the ones mentioned in Chapter 1, show how important it is to understand the role that certain factors such as blood velocity, blood pressure, and wall shear stress may play in the development of atherosclerotic lesions at certain locations in the aorta. However, most of these studies have modeled the aorta as a rigid artery instead of an elastic one. As Pedersen *et al.* (1993) stated in one of their studies regarding the use of rigid models, "This is likely to induce minor errors while estimating absolute values for wall shear stress, as elasticity has been reported to reduce the maximal shear stress level" [see also Liepsch (1986)]. Although these errors may only be minor, it is important to understand the effect of elasticity. In this study, blood flow through a rigid model of the aorta will be compared to that of an elastic model in order to better understand what effects elasticity may have on the wall shear stress, blood velocity, and blood pressure under different blood flow conditions. The effect that each of the arterial branch flows has on these properties will also be studied.

2.1 Basic Fluid Mechanics

Blood vessels are essentially circular pipes, whose impermeable wall is composed of cells and cell products, with an incompressible liquid, blood, flowing through them. When a liquid flows through a pipe, viscous forces resist its motion. These forces are maximum at the wall and decrease in magnitude as the distance, y, from the boundary increases. Because of the presence of viscous resistance, the velocity profile has a maximum at the center of the pipe and decreases near the wall. Fluid particles immediately adjacent to the wall are assumed to be at rest (no-slip condition). The radial difference in velocity shears the flow with the velocity gradient and rate of shear being maximum at the wall and decreasing as the distance from the boundary increases. Since there is a velocity gradient, du/dy, work must be done between the adjacent layers of liquid particles that slide over each other in order to overcome viscous resistance between them. The shear stress, or tangential force per unit area, τ, represents a measure of this work. In the case of a Newtonian liquid which obeys Newton's law of viscosity, the shear stress is linearly related to the rate of shear (Lelkes 1999):

$$\tau = \mu \frac{du}{dy} \tag{2.1}$$

where the dynamic viscosity, μ, is a property of the liquid. However, the linear relationship between the shear stress and rate of shear in Equation 2.1 does not hold true for a liquid such as whole blood, which is considered in essence to be a non-Newtonian fluid for two reasons: 1) Blood needs a small initial yield stress, τ_o, to begin flowing 2) There is a non-linear relationship between τ and du/dy at low shear rates of approximately 20 1/s (Patel and Vaishnav 1980). However, at high shear rates (from 200-300 1/s up to >1000 1/s) typically seen in large blood vessels (>0.5 mm in diameter), the blood acts more like a Newtonian fluid. Although the blood does not always remain Newtonian throughout the pulsation cycle, for all practical purposes it can be considered a homogenous Newtonian

16

continuum having a viscosity of 0.03 Poise (Ku 1997) at 37°C (Lelkes 1999). Equation 2.1 can still model shear stress within non-Newtonian blood, provided that the coefficient of viscosity varies as a suitable decreasing function of shear rate du/dy (Fung 1997).

2.2 The Vascular System

The blood is the main working fluid throughout the entire vascular system. The vascular system is composed of two separate circuits: the pulmonary circulation, which fills the lungs with blood pumped from the right side of the heart, and the systemic circulation, which fills vascular beds throughout the body with oxygenated blood that has returned from the lungs to the left side of the heart (Patel and Vaishnav 1980). A healthy individual at any given time circulates about 5-5.5 L of blood. From this volume of blood, 11% is distributed to the pulmonary network, 82% to the systemic network and 7% to the heart and its vessels. Within the systemic network, 16% of the total blood volume is held by the aorta and arterial tree, 4% by the capillaries, and 60% or more by the veins (Lelkes 1999). Each of the two separate circuits have three components: the arteries, which carry blood away from the heart; the capillaries, which exchange oxygen, CO_2, and metabolites between the blood and tissues; and the veins, which return deoxygenated blood back to the heart from the capillaries. The structure of each of these three components differs according to the role they play in circulation. For instance, the vessel walls are thicker in the systemic circulation than in the pulmonary circulation since the pulmonary circulation is a much lower pressure system (Patel and Vaishnav 1980).

17

2.3 Hemodynamic Forces On The Vessel Wall

The flow of blood through the arteries, such as the aorta, has been studied for several years. However, despite all of the research that has been carried out, it is not clear as to whether the blood flow through the arteries is normally disturbed or fully turbulent. It has been found that, during the start of systole until the end of the acceleration phase, the velocity waveforms in the aorta do not have high-frequency components which indicates that the flow during this phase of the cardiac cycle may be laminar. However, during the deceleration phase which occurs past the peak of systole, the velocity waveforms contain high-frequency fluctuations that are due to flow disturbances (Nerem and Seed 1972). A spectral analysis performed on these high-frequency fluctuations has lead researchers to believe that the blood flow during this phase of the cardiac cycle is in fact turbulent. This is an important finding since atherosclerotic plaques have often been found at turbulent flow sites in the aorta (Fung 1997). Whether the flow through the aorta is highly disturbed, transitional, or turbulent, hemodynamic forces due to the flow pulsatility are exerted on the aortic vessel wall.

The forces that the flowing blood exerts on the vasculature are viscous friction and distension, two mutually orthogonal components. The friction force per unit area, which is exerted tangentially to the wall, is known as the wall shear stress and the distending force per unit area, which acts on the wall perpendicularly and is essentially equal to the fluid pressure, is known as normal stress. Both of these forces act on the wall macroscopically and microscopically. For instance, macroscopically, the pressure and shear stress create longitudinal and circumferential (hoop) strains by stretching and distending the wall. The longitudinal strain is carried mostly by the adventitia and the vascular side branches while the subendothelial layer carries some of the circumferential strain and the tunica media carries most of it. Microscopically, the wall shear stress and friction forces are applied

18

directly to the individual endothelial cells, shearing and pressing their luminal surface and stretching their basement membrane (Lelkes 1999). It has also been found in a recent study by Noria *et al.* (2004) that the endothelial cells elongate and align in the direction of the shear stress through a mechanism that involves the growth, fusion, and reorientation of stress fibers. They found that the sensitivity of the endothelial cells to the shear stress may be a factor in the growth of atherosclerotic lesions. This study, along with the previous studies, have shown these forces may play an important role in the development of atherosclerotic lesions in the aorta.

2.4   Overview of Aorta

The aorta originates in the left ventricle of the heart at the aortic valve and serves as the main trunk of the entire systemic arterial system, as shown in **Figure 2.1**. It is approximately 30 cm in length, and is divided into three sections: the ascending aorta, aortic arch, and descending aorta, which is made up of the thoracic and abdominal aorta (Koehler 1996). The ascending aorta, which makes up the first few centimeters of the aorta, carries blood up and out of the left ventricle. The aorta then makes a 180° turn over the arch of the aorta or aortic arch. The radius of curvature at the aortic arch is approximately 500 mm (Moore 1991). Blood flows down the arch through the descending aorta. The first segment of the descending aorta is the thoracic aorta which has a diameter of approximately 25.3 mm and has several arteries branching from it. From here, blood travels to the last region, the abdominal aorta. The diameter of the abdominal aorta varies from person to person and is between 21.5 mm and 26.9 mm. Like the thoracic section, the abdominal aorta has several arterial branches. The aorta tapers down to approximately 18 mm before bifurcating into the left and right common iliac arteries (Thibodeau and Patton 1996).
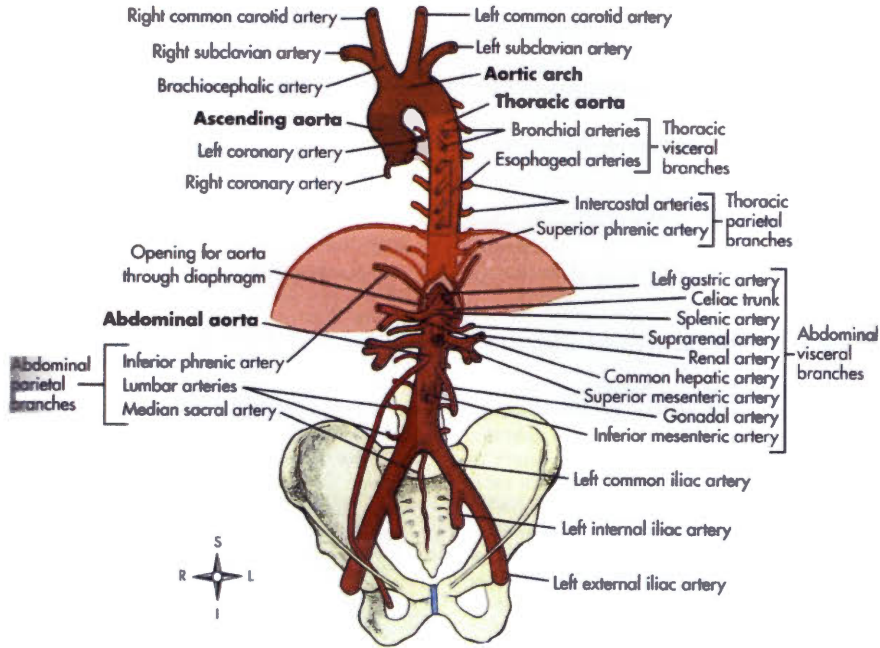
Figure 2.1: *Diagram of the Aorta (Thibodeau and Patton 1996).*

Overall, the change in the area of the aorta due to tapering fits the exponential equation,

$$A(x) = A_{in}e^{-kx} \tag{2.2}$$

where $A(x)$ is referred to in the present study as the anatomical area, with $A_{in} = \pi D_{in}^2/4$ the area at the upstream site, x the distance from the upstream site, and k the taper factor (Fung 1997).

2.5   Basic Equations of Flow - Governing Equations

When the temperature distribution within a flow field of an incompressible fluid, such as blood, is uniform and constant, two basic laws govern the motion of the fluid particles: conservation of mass and Newton's Second Law of Motion. These two equations can be used to develop other equations that govern the motion of fluid particles (Patel and

20

Vaishnav 1980).

2.5.1 Conservation of Mass

The conservation of mass,

$$\frac{dm}{dt} = \sum \dot{m}_{in} - \sum \dot{m}_{out}, \tag{2.3}$$

states that the rate of change of mass present in a control volume is equal to the difference between the sum of the mass flows entering and exiting the control volume. This law is physically very obvious but places certain constraints on the distributions of velocity that can exist in any given flow situation. For instance, the amount of mass that flows into a tube must equal the amount flowing out of the tube, unless the mass inside the tube varies in time. Although the density of all real fluids can change to some extent, liquids such as water and blood can be approximated as being incompressible. When blood is flowing through a rigid tube, the term $dm/dt = 0$. Therefore, the mass of blood that enters the tube must be equal to the mass of blood exiting the tube even when the tube tapers (Caro *et al.* 1978). In this case Equation 2.3 reduces to

$$\sum (V_i A_i)_{in} = \sum (V_i A_i)_{out}$$
$$\sum Q_{in} = \sum Q_{out} \tag{2.4}$$

where $Q = V_i A_i$ is the volumetric flow rate of blood passing through a given section of the aorta. However, when blood is flowing through an elastic tube, the cross-sectional area, A, can vary with time and Equation 2.3 becomes

$$\frac{\partial A}{\partial t} + \frac{\partial Q}{\partial x} + q = 0 \tag{2.5}$$

as derived by Iannelli from the Reynolds Transport Theorem, as shown in Appendix A.

2.5.2 Newton's Second Law of Motion

Newton's Second Law of Motion, or the conservation of linear momentum, states that for a fluid particle in motion relative to an inertial coordinate system, the sum of all the external forces acting on the particle is equal to the product of the mass and the absolute acceleration of the particle:

$$\sum F = ma \tag{2.6}$$

where m is the mass of the particle, a is the particle acceleration, and F is the resultant external forces acting on the particle. The resultant forces acting on the particle are: 1) the gravitational force, 2) pressure forces, and 3) viscous forces due to internal friction within the fluid (Patel and Vaishnav 1980). Using a control volume analysis for an incompressible Newtonian fluid such as blood, Equation 2.6 becomes

$$\frac{\partial Q}{\partial t} + \frac{\partial}{\partial x}\left(\frac{Q^2}{A}\right) + \frac{A}{\rho}\frac{\partial P}{\partial x} = -\frac{Q^2 f_D}{2AD_h} + gA. \tag{2.7}$$

2.5.3 The Bernoulli Equation

The different pressures that a fluid element may experience and the different vertical locations relative to a reference plane it may occupy determine the velocity of the element (Patel and Vaishnav 1980). The relation that exists between the pressure, velocity, and elevation of a element within a inviscid, incompressible steady fluid which is moving between two locations along a streamline is given by the Bernoulli equation

$$\frac{P_1}{\rho g} + \frac{V_1^2}{2g} + z_1 = \frac{P_2}{\rho g} + \frac{V_2^2}{2g} + z_2 = \text{constant} \tag{2.8}$$

which originates from the integration of Equation 2.7 where P_1 and P_2 are the pressures at locations 1 and 2, z_1 and z_2 are the elevations of the locations, and V_1 and V_2 are the fluid velocities at these locations. However, blood is not a inviscid fluid; therefore, there

22

will be a pressure drop (head loss) as the blood moves through a vessel. For fully developed, incompressible flow, this pressure loss can be quantified using the Darcy-Weisbach equation:

$$h_f = f \frac{L}{D} \frac{V^2}{2g} \qquad (2.9)$$

where L is the distance between locations 1 and 2, D is the diameter of the tube, V is the velocity of the fluid, g the gravitational acceleration, and f is the Darcy friction factor given by the Colebrook formula

$$\frac{1}{\sqrt{f}} = -2.0 \log \left(\frac{\varepsilon/D}{3.7} + \frac{2.51}{Re\sqrt{f}} \right) \qquad (2.10)$$

where ε/D is a measure of the surface roughness of the interior of the aortic arterial wall (White 1986). With the addition of Equation 2.9, the Bernoulli equation becomes the generalized energy equation

$$\frac{P_1}{\rho g} + \frac{V_1^2}{2g} + z_1 = \frac{P_2}{\rho g} + \frac{V_2^2}{2g} + z_2 + f \frac{L}{D} \frac{V^2}{2g} \qquad (2.11)$$

which, in this form, models the flow of blood within a straight rigid tube.

2.6 Aorta Model Used In Present Study

For the present study an analytical, finite-element model was developed to simulate blood flow through the aorta. Unlike rigid glass models which have been used in many previous studies, the analytical model developed in the current study can simulate the vessel as being either rigid or elastic. Although this model can be used to simulate blood flow through any blood vessel, the current study focuses only on the abdominal aorta since it is the more prone to the development of atherosclerotic lesions.

In this study, four different models of the aorta will be presented. The first model will represent the aorta as being a straight rigid artery and the second model will represent the

aorta as being a straight elastic artery. The third model will represent the aorta as being a tapered rigid artery and the fourth model will represent the aorta as being a tapered elastic artery. The effects of the arterial branch flows will also be investigated.

Throughout this study the aorta was modeled using 50 nodes (49 elements). For the cases without branch flows, a uniform mesh was used. A non-uniform mesh that requires a node at the center of each branch location was used for the cases with branch flows. For each model it was assumed that the individual was lying down (thus the aorta was aligned horizontally) and therefore gravitational effects on the blood flow were not investigated in this study.

2.6.1   Model Parameters

The analytical model requires the following input parameters: the density and viscosity of blood; the inlet diameter, wall thickness and modulus of elasticity of the abdominal aortic wall; height of aortic-wall endothelial cells; taper factor; gravitational acceleration; and blood pressure at the inlet and outlet of the abdominal aorta. The parameter values used in this study are shown in **Table 2.1**. The roughness of the inner flow surface of the aorta was taken as the height of the endothelial cells, which form the inner layer of the aortic wall and come in direct contact with the blood flow. The endothelial cell height was measured from cultured cells using the graticule of a microscope in the Biomedical Engineering laboratory of Dr. Anthony English at the University of Tennessee, Knoxville. The taper factor for the abdominal aorta was calculated using Equation 2.2 and measurements of the inlet and outlet diameters of the abdominal aorta cited by Moore and Ku (1994a) as shown in Appendix B. Values for the remaining parameters were taken from literature as referenced in **Table 2.1**.

24

Blood Density	$\rho = 1050.0$ kg/m^3	(Porenta *et al.* 1986)
Blood Viscosity	$\mu = 0.003$ N·s/m^2	(McDonald 1974)
Abdominal Aorta Inlet Diameter	$D_{in} = 0.025$ m	(Moore and Ku 1994a)
Abdominal Aorta Wall Thickness	$t = 0.0015$ m	(Geneser 1986)
Modulus of Elasticity for Aorta	$E = 4.4 \times 10^5$ Pa	(Bergel 1961)
Endothelial Cell Height	$\varepsilon = 1.25 \times 10^{-6}$ m	(Lab experiment)
Taper Factor	$k = 0.0$ 1/m for straight $k = 3.4$ 1/m for tapered	(Calculated)
Gravitational Acceleration	$g = 9.81$ m/s	(Physics)
Blood Pressure	$P_{in} = 100$ mm Hg at inlet $P_{out} = 97$ mm Hg at outlet	(Thibodeau and Patton 1996)

2.6.2   Model Geometry

The model must include the physical geometry of the abdominal aorta. Physical dimensions of the aorta as given in Section 2.6.1 are used in the following equation to determine the anatomical area of the aorta at each node i:

$$A_{anat,i} = A_{in}\, e^{-kx_i}. \tag{2.12}$$

This study also considers the effect of blood leaving the abdominal aorta through seven major aortic branches: the celiac, superior mesenteric, right and left renal, inferior mesenteric, and the right and left iliac arteries. The location and diameter of each branch, as well as the percentage of the total blood flow rate of the abdominal aorta which flows through each of the branches are given in **Table 2.2**. The flow rates given in **Table 2.2** represent the average of values taken from literature (Moore 1991; Pedersen *et al.* 1993; Lee and Chen 2002).

Table 2.2: *Location, diameter, and percentage of total blood flow rate through abdominal aorta carried by each branch.*

Abdominal Aortic Branches	Location of Branch Center Downstream from Abdominal Aorta Inlet (m)	Diameter of Branch (m)	Percentage of Abdominal Aorta Blood Flow Rate Carried by the Branch
Celiac	0.037	0.008	21.24%
Superior Mesenteric	0.053	0.008	14.66%
Right Renal	0.069	0.006	14.66%
Left Renal	0.072	0.006	14.66%
Inferior Mesenteric	0.143	0.006	4.77%
Right Iliac	0.193	0.013	15.01%
Left Iliac	0.193	0.013	15.01%

2.6.3   Least-squares Solver Routine

The principal variables in the model are the blood pressure and velocity. For the 50 nodes of the developed model there are 100 unknowns: 50 nodal velocities and 50 nodal pressures, but 98 equations for these variables exist: 49 nodal continuity equations and 49 nodal energy equations. The required additional two pieces of information are the boundary inlet and outlet pressures. The model requires the input of initial guesses for the blood flow velocity at the inlet node; the Darcy friction factor, f, at all nodes; and the blood pressure at all interior nodes. The first step in the iteration loop is to determine the physiological area of the aorta (the area of the aorta after its walls expand due to elasticity and the blood pressure within the abdominal aorta) at each node i based on the pressure value, P_i, that was determined in the previous iteration using the equation

$$A_i = A_{anat,i} \left(1 + C_{e/r} \frac{P_i r_{anat,i}}{Et_h}\right)^2 \tag{2.13}$$

that results from an incrementally linear elastic module for the arterial wall where $A_{anat,i}$ and $r_{anat,i}$ are the anatomical area (unstretched area of aorta) and radius at node i, respec-

26

tively; E is the modulus of elasticity for the aortic wall; and t_h is the thickness of the aortic wall. The term $C_{e/r}$ in Equation 2.13 is a "flag" that is used to indicate whether the aorta is to be considered as elastic ($C_{e/r} = 1$) or rigid ($C_{e/r} = 0$ — in which case, the physiological area will be equal to the anatomical area). The blood flow velocity at the interior nodes and exit node are then determined from the previous estimate of inlet velocity and the physiological area from the conservation of mass using the equation

$$V_i = \frac{V_{in}A_{in}}{A_i}\left(1 - \sum q_B\right) \tag{2.14}$$

where q_B are the volumetric flow rates of each arterial branch expressed as a percentage of the total flow rate.

The iteration loop then evaluates three residual terms, R_f, R_P and R_V. The friction-factor residual,

$$R_{f,i}^2 = \left(\frac{1}{\sqrt{f_i}} + 2.0\log\left(\frac{\varepsilon/D_i}{3.7} + \frac{2.51}{Re_i\sqrt{f_i}}\right)\right)^2, \tag{2.15}$$

is based on Equation 2.10 and evaluated at all nodes to refine the initial guesses for the Darcy friction factor, f_i, at each node. The pressure residual,

$$R_{P,i}^2 = \left(\frac{\dot{m}_{in}P_{in} - \dot{m}_i P_i}{\rho g} + \frac{\dot{m}_{in}V_{in}^2 - \dot{m}_i V_i^2}{2g} + (\dot{m}_{in}z_{in} - \dot{m}_i z_i)\right.$$
$$\left. - \int_{x_{in}}^{x_i}\left(\frac{V_B^2}{2g} + z_B + \frac{P_B}{\rho g}\right)d\dot{m}_B - \int_{x_{in}}^{x_i}\frac{\dot{m}_i f_i V_i^2}{2D_i g}dx\right)^2, \tag{2.16}$$

is based on the conservation of energy and conservation of linear momentum. The terms in Equation 2.16 respectively represent the pressure drop, the change in kinetic energy, the change in potential energy, the energy transported out of the aorta with the branch blood flows, and the friction loss. The pressure residual is evaluated between the inlet of the abdominal aorta and each interior node to refine the initial guesses for blood pressure. The inlet velocity residual

$$R_V^2 = \left(\frac{\dot{m}_{in}P_{in} - \dot{m}_{out}P_{out}}{\rho g} + \frac{\dot{m}_{in}V_{in}^2 - \dot{m}_{out}V_{out}^2}{2g} + (\dot{m}_{in}z_{in} - \dot{m}_{out}z_{out})\right.$$
$$\left. - \int_{x_{in}}^{x_{out}}\left(\frac{V_B^2}{2g} + z_B + \frac{P_B}{\rho g}\right)d\dot{m}_B - \int_{x_{in}}^{x_{out}}\frac{\dot{m}_i f_i V_i^2}{2D_i g}dx\right)^2, \tag{2.17}$$

is the same equation as the pressure residual but evaluated between the inlet and exit of the abdominal aorta to determine the inlet velocity based on the prescribed inlet and outlet pressure boundary conditions. The iteration loop uses a least-squares method to minimize the total residual, R_{total}, given by

$$R_{total}^2 = \sum_{i=1}^{N} R_{f,i}^2 + \sum_{i=2}^{N-1} R_{P,i}^2 + R_V^2 \tag{2.18}$$

where N is the number of nodes in the model (throughout this study, $N = 50$). Each iteration generates refined estimates for the blood flow velocity, V_{in}, at the inlet node; the Darcy friction factor, f_i, at all nodes; and the blood pressure, P_i, at all interior nodes. Since the model involves the same number of equations (including the two pressure boundary conditions) and unknowns, the least-squares method will lead to the exact solution, which is accurately determined by driving the total residual to machine zero.

Chapter 3

Results

3.1 Analysis of Aorta Neglecting Branch Flows

In this study, four analytical models of the abdominal aorta are presented as mentioned in Section 2.6. The first model represents the abdominal aorta as being a straight rigid artery, the second a straight elastic artery, the third a tapered rigid artery, and the fourth a tapered elastic artery. Each of these four models represent the abdominal aorta as having no branch flows.
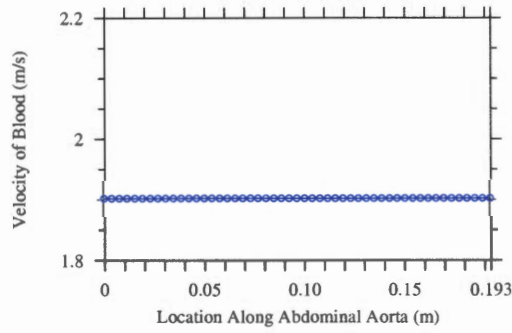
3.1.1 Straight Rigid Artery Model

Figure 3.1 shows how the diameter, blood pressure, blood velocity, and wall shear stress vary along the length of the abdominal aorta (0.193 m) when the aorta is modeled as a straight rigid artery with no branch flows. In this case, the anatomical diameter of the abdominal aorta is a constant 0.025 m throughout its total length. Since the abdominal aorta is rigid in this model, it cannot expand; therefore, the anatomical diameter and physiological diameter are equal as shown in **Figure 3.1(a)**. The blood flow velocity was also found to be constant along the length of the abdominal aorta, as shown in **Figure 3.1(c)**. This
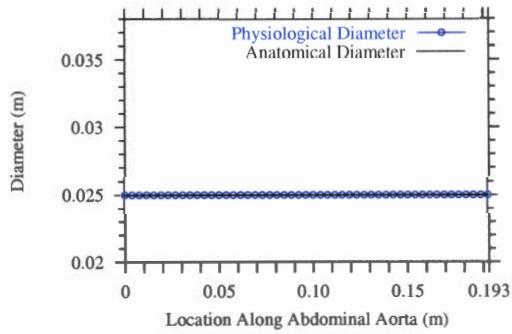
(a) Physiological Diameter
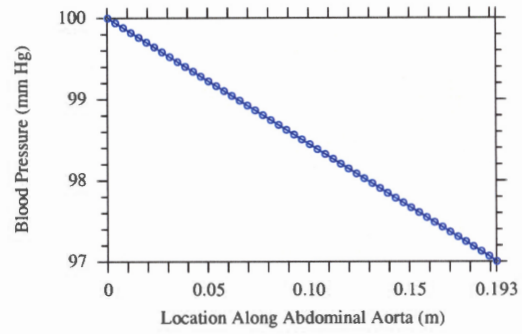
(b) Blood Pressure

(c) Velocity of Blood
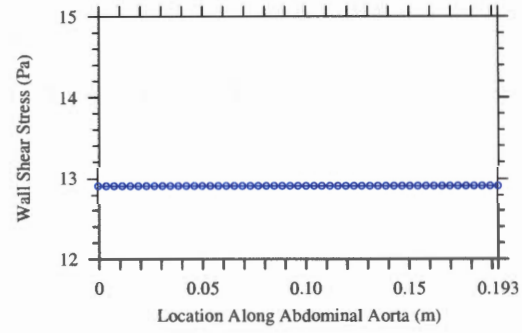
(d) Wall Shear Stress

Figure 3.1: *Results for the Straight Rigid Artery Model.*

30

result is expected since the conservation of mass states that, for steady flow, the mass flow rate is constant; therefore, the density and flow area are constant, the velocity must also be constant. The blood pressure was found to decrease linearly along the length of the abdominal aorta, as shown in **Figure 3.1(b)**. Since velocity is constant along the abdominal aorta when modeled as a straight rigid artery, the energy equation (Equation 2.11) reduces to

$$\frac{P_{in} - P_i}{\rho g} = f \frac{x_i}{D_i} \frac{V_i^2}{2g}. \tag{3.1}$$

Therefore, the pressure drop along the aorta is linear as given by the equation

$$\Delta P_i = \frac{\rho f V_i^2}{2D_i} x_i = C x_i. \tag{3.2}$$

Like the diameter and velocity, the wall shear stress is constant along the length of the abdominal aorta as shown in **Figure 3.1(d)**. This is also expected since all the terms on the right hand side of the following equation are constant

$$\tau_w = \frac{f \rho V_i^2}{8}. \tag{3.3}$$
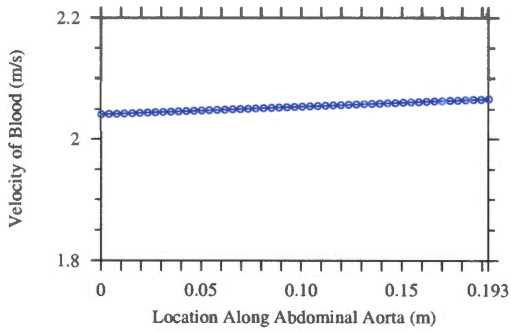
3.1.2 Straight Elastic Artery Model

Figure 3.2 shows how the diameter, blood pressure, blood velocity, and wall shear stress vary along the length of the abdominal aorta when the aorta is modeled as a straight elastic artery with no branch flows. Like the previous case in which the aorta was modeled as a straight rigid artery, the anatomical diameter is constant along the length of the abdominal aorta as shown in **Figure 3.2(a)**. However, since the elasticity of the aorta wall is accounted for in this model, the blood pressure causes the abdominal aorta walls to expand resulting in a physiological diameter that is greater than the anatomical diameter. The physiological diameter decreases along the length of the abdominal aorta as the blood pressure decreases as shown in **Figure 3.2(b)**. In accordance with the energy equation,
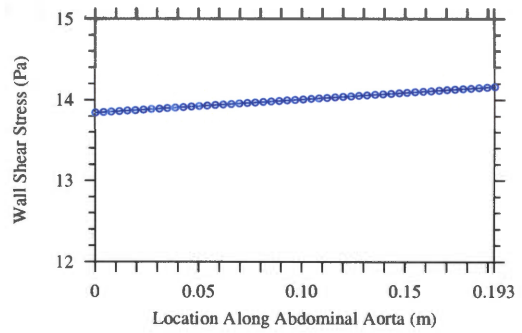
31
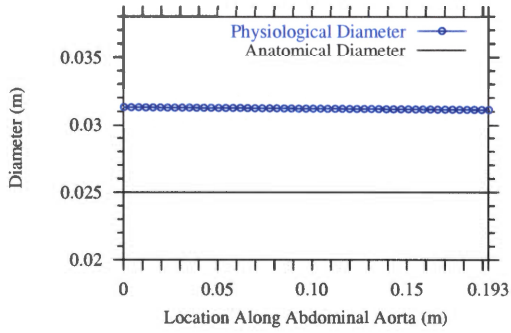
(a) Physiological Diameter
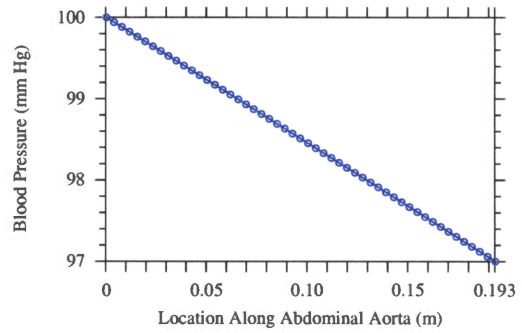
(b) Blood Pressure
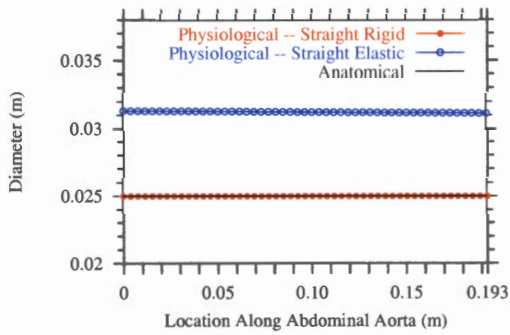
(c) Velocity of Blood

(d) Wall Shear Stress

Figure 3.2: *Results for the Straight Elastic Artery Model.*

this decrease in blood pressure is a result of the increase in velocity which in turn occurs due to the decrease in flow area. Since there is an increase in velocity, the wall shear stress increases according to Equation 3.3. Note that the wall shear stress is also affected by the decrease in the diameter since f in Equation 3.3 is a function of Reynolds number; however, this effect is very small compared to the effect of velocity. Although the four parameters discussed appear to vary linearly along the length of the abdominal aorta in **Figure 3.2**, they are actually non-linear.

3.1.3   Comparison of Results for the Straight Rigid and Straight Elastic Artery Models

Figure 3.3 provides a direct comparison of the results for the straight rigid artery model and straight elastic artery model. As discussed above, the physiological diameter of the straight rigid model is the same as the anatomical diameter. For the straight elastic model, the physiological diameter is allowed to expand as shown in **Figure 3.3(a)**. In this study, the blood pressure is assumed to drop from 100 mmHg to 97 mmHg over the length of the abdominal aorta. As mentioned above, the velocity is constant for the straight rigid model; therefore, the blood pressure drop is linear between the inlet and exit. For the straight elastic model, the blood pressure drop is non-linear; however, this difference is very small compared to the overall pressure drop through the abdominal aorta and thus is not easily seen in **Figure 3.3(b)** due to the scale of the graph.
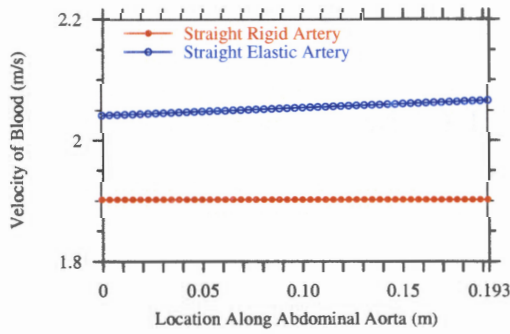
The model determines the velocity at the inlet of the abdominal aorta by minimizing the velocity residual given by Equation 2.17. This equation is obtained by writing the energy equation between the inlet and exit of the abdominal aorta. This yields an equation
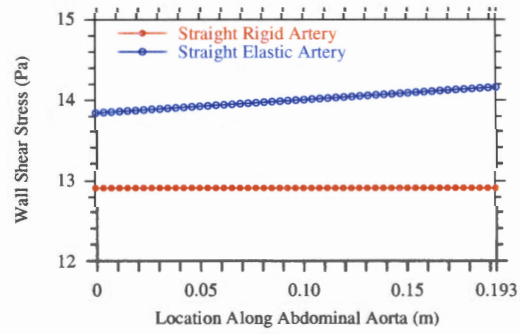
33

(a) Physiological Diameter
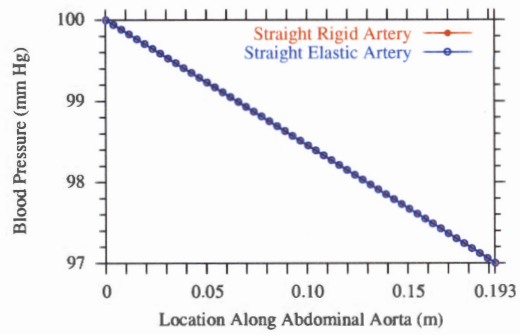
(b) Blood Pressure

(c) Velocity of Blood

(d) Wall Shear Stress

Figure 3.3: *Comparison of Results for the Straight Rigid and Straight Elastic Artery Models.*

34

for the inlet velocity of the form

$$V_{in}^2 = \frac{P_{out} - P_{in}}{\rho g \left[1 - \left(1 + \frac{fL}{2gD} \right) \frac{A_{in}^2}{A_{out}^2} \right]} \tag{3.4}$$

since $V_{out} = V_{in} A_{in}/A_{out}$. The total pressure drop across the length of the abdominal aorta is maintained at the same value in both the straight rigid and the straight elastic model; therefore, the ratio of the square of the inlet velocities for the two models is given by

$$\frac{V_{in}^2\big|_{rigid}}{V_{in}^2\big|_{elastic}} = \frac{1 - \left(1 + \frac{fL}{2gD} \right) \frac{A_{in}^2}{A_{out}^2}\big|_{elastic}}{-\frac{fL}{2gD}\big|_{rigid}} \tag{3.5}$$

since the area is constant in the rigid model. As seen in **Figure 3.2(a)** for the elastic case, $A_{in} \approx A_{out}$. Making this approximation, Equation 3.5 reduces to

$$\frac{V_{in}^2\big|_{rigid}}{V_{in}^2\big|_{elastic}} \approx \frac{f_{elastic}}{f_{rigid}} \frac{D_{rigid}}{D_{elastic}}. \tag{3.6}$$

The terms in the denominator of the right-hand side of Equation 3.6 are greater than the terms in the numerator; therefore, the inlet velocity for the straight elastic model must be greater than the inlet velocity for the straight rigid model. The results shown in **Figure 3.3(c)** agree with this assessment. This increase in velocity for the straight elastic case is directly responsible for the increase in wall shear stress seen in **Figure 3.3(d)**.
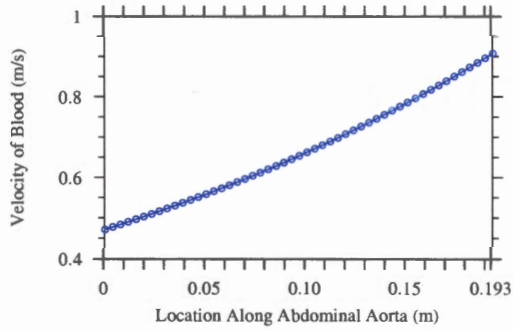
3.1.4 Tapered Rigid Artery Model

Figure 3.4 shows how the diameter, blood pressure, blood velocity, and wall shear stress vary along the length of the abdominal aorta when the aorta is modeled as a tapered rigid artery with no branch flows. In this model, the anatomical diameter gradually decreases along the length of the abdominal aorta according to Equation 2.12. This more realistically matches the actual shape of the aorta than does the straight model. Since the abdominal aorta is modeled as rigid instead of elastic, it is not allowed to expand; therefore, the
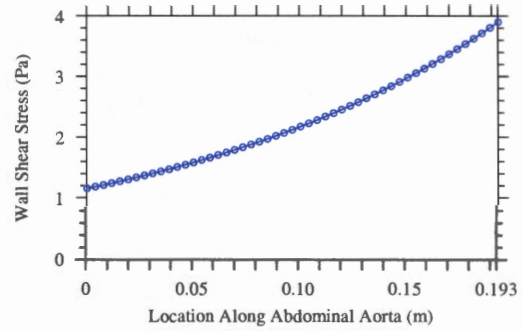
35
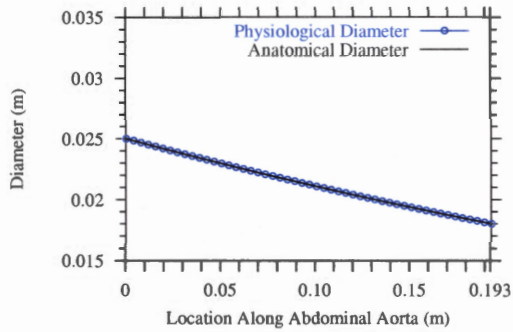
(a) Physiological Diameter
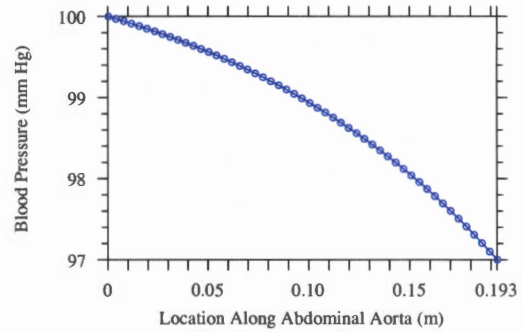
(b) Blood Pressure

(c) Velocity of Blood

(d) Wall Shear Stress

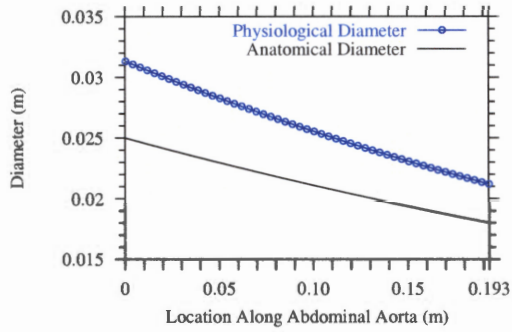**Figure 3.4:** *Results for the Tapered Rigid Artery Model.*

anatomical and physiological diameters are equal. As shown in **Figure 3.4(c)**, velocity increases as area decreases along the length of the abdominal aorta due to the conservation of mass. Due to the fact that the decrease in area along the length is non-linear, the increase in velocity is also non-linear. The increase in velocity causes there to be an increase in wall shear stress as shown in **Figure 3.4(d)** according to Equation 3.3 and a decrease in pressure as shown in **Figure 3.4(b)** according to the energy equation.
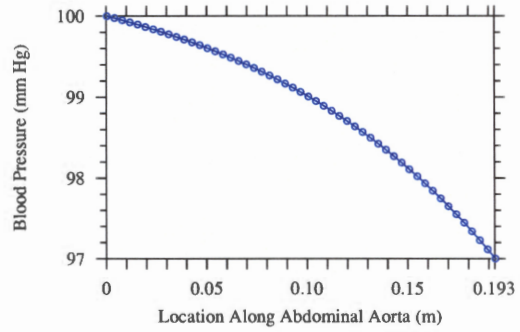
3.1.5 Tapered Elastic Artery Model

Figure 3.5 shows how the diameter, blood pressure, blood velocity, and wall shear stress vary along the length of the abdominal aorta when the aorta is modeled as a tapered elastic artery with no branch flows. As shown in **Figure 3.5(a)**, the anatomical diameter decreases along the length of the abdominal aorta according to Equation 2.12. Due to its elasticity the artery is able to expand; therefore, the physiological diameter is larger than the anatomical diameter. The physiological diameter expands more at the inlet than exit due to the higher pressure at the inlet. As with the previous model, the velocity increases along the length of the abdominal aorta since area decreases as shown in **Figure 3.5(c)**. The increase in velocity causes there to be an increase in wall shear stress as shown in **Figure 3.5(d)** according to Equation 3.3 and a decrease in pressure as shown in **Figure 3.5(b)** according to the energy equation.

3.1.6 Comparison of Results for the Tapered Rigid and Tapered Elastic Artery Models
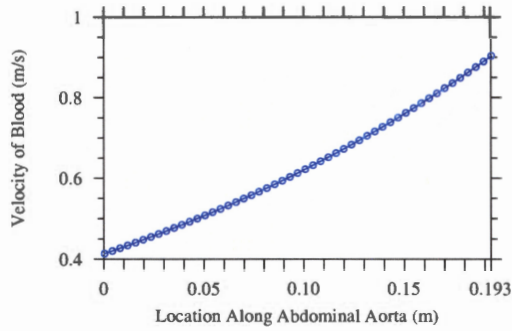
Figure 3.6 provides a direct comparison of the results for the tapered rigid artery model and tapered elastic artery model. As discussed above, the physiological diameter for the tapered rigid model is the same as the anatomical diameter and is given by Equation 2.12.
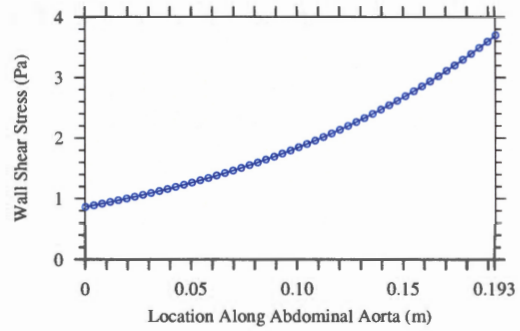
37

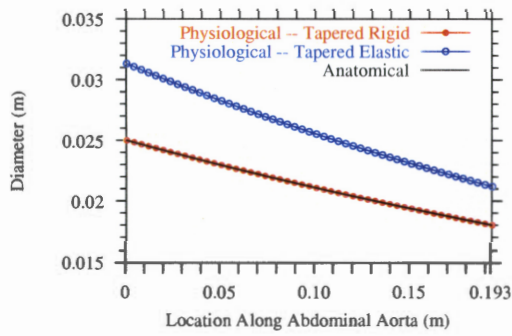(a) Physiological Diameter

(b) Blood Pressure
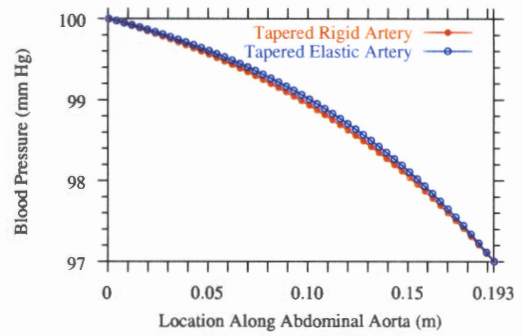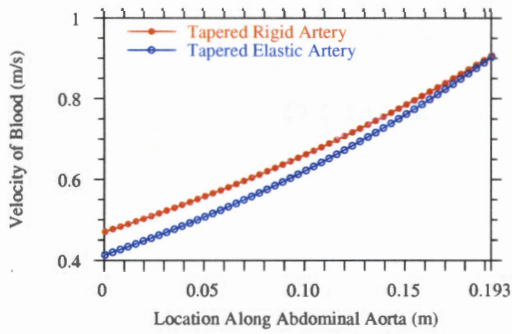
(c) Velocity of Blood

(d) Wall Shear Stress

Figure 3.5: *Results for the Tapered Elastic Artery Model.*
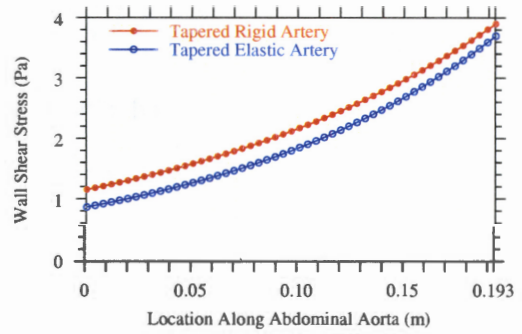
(a) Physiological Diameter

(b) Blood Pressure

(c) Velocity of Blood

(d) Wall Shear Stress

Figure 3.6: *Comparison of Results for the Tapered Rigid and Tapered Elastic Artery Models.*

For the tapered elastic model the physiological diameter is allowed to expand as shown in **Figure 3.6(a)**.

As discussed above in Section 3.1.3, the velocity at the inlet of the abdominal aorta is determined by Equation 3.4. In this study the blood pressure is assumed to drop from 100 mmHg to 97 mmHg over the length of the abdominal aorta; therefore, the ratio of the square of the inlet velocities for the two tapered models is given by

$$
\frac{V_{in}^2\big|_{rigid}}{V_{in}^2\big|_{elastic}} = \frac{1 - \left(1 + \frac{fL}{2gD}\right)\frac{A_{in}^2}{A_{out}^2}\big|_{elastic}}{1 - \left(1 + \frac{fL}{2gD}\right)\frac{A_{in}^2}{A_{out}^2}\big|_{rigid}}
\tag{3.7}
$$

which cannot be simplified as it was before for the straight rigid and straight elastic models. However, the area ratios in Equation 3.7 are the dominant terms. The decrease in the physiological diameter over the length of the abdominal aorta is greater for the tapered elastic model than for the tapered rigid model as shown in **Figure 3.6(a)**; therefore, the area ratio for elastic will be greater than the area ratio for rigid in Equation 3.7. As a result, the inlet velocity for the tapered rigid model will tend to be greater than for the tapered elastic model which agrees with the results shown in **Figure 3.6(c)**. Due to the fact that the velocity for the tapered rigid model is higher than for the tapered elastic model, the blood pressure is lower and the wall shear stress is higher for the rigid model as shown in **Figures 3.6(b)** and **3.6(d)**, respectively.

3.1.7   Comparison of Results for the Straight and Tapered Models

The importance of including taper in a model of the abdominal aorta can be seen by comparing the results for the straight models (**Figure 3.3**) to those of the tapered models (**Figure 3.6**). For the straight models, the velocity is high and relatively constant along the length of the abdominal aorta. When taper is included in the models, the velocity is considerably lower and increases dramatically along the length of the abdominal aorta

40

due to the decrease in diameter. The decrease in velocity results in an even more dramatic decrease in wall shear stress for the tapered models. Also, for the straight models, the velocity for the elastic model is greater than it is for the rigid model. However, when taper is included, the rigid model predicts a higher velocity than the elastic model. The reason for this difference can be seen by considering Equations 3.6 and 3.7. Due to the taper, the area ratios dominate Equation 3.7. For the straight models, the area ratios are equal to or approximately equal to one and Equation 3.6 is dominated by the elastic-to-rigid ratio for the Darcy friction factor and diameter of the abdominal aorta.
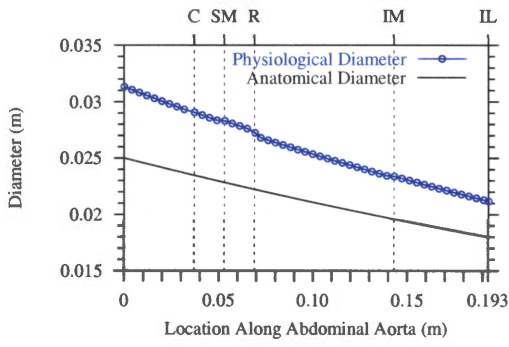
3.1.8 Tapered Elastic Artery Model With Branch Flows

It is seen from the previous models that do not account for branch flows that taper and elasticity have a significant effect on the model predictions; therefore, for the study that was performed in which the branch flows were included, it was only necessary to consider the tapered elastic artery model. It is also obvious that this model is a better representation of the abdominal aorta since this vessel is a tapered elastic artery.

Figure 3.7 shows how the diameter, blood pressure, blood velocity, and wall shear stress vary along the length of the abdominal aorta when the aorta is modeled as a tapered elastic artery with branch flows. In **Figure 3.7(a)** it is seen that the physiological diameter is greater than the anatomical diameter since the artery is able to expand. It can also be seen from this figure that the physiological diameter changes suddenly at the locations along the length of the abdominal aorta where there is a branch. This sudden change is due to the increase or decrease in the blood pressure at these locations as seen in **Figure 3.7(b)**.

The velocity of the blood flow along the length of the abdominal aorta is shown in **Figure 3.7(c)**. Between the branches the velocity increases according to conservation of mass due to the taper of the aorta. At the branch locations the velocity decreases due to the
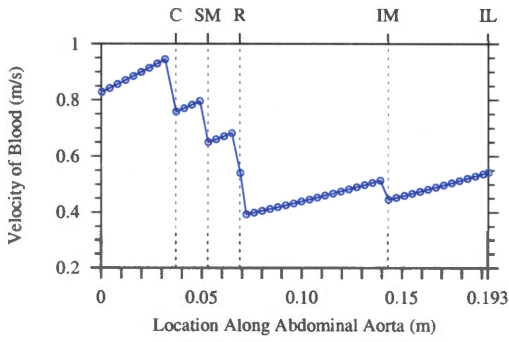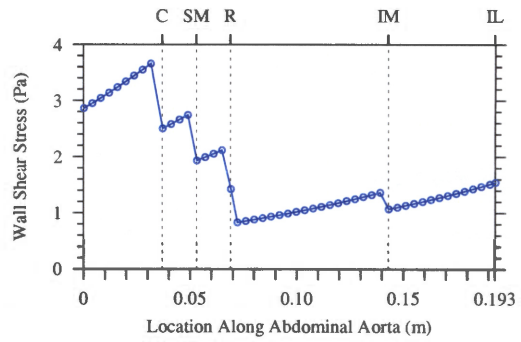
41

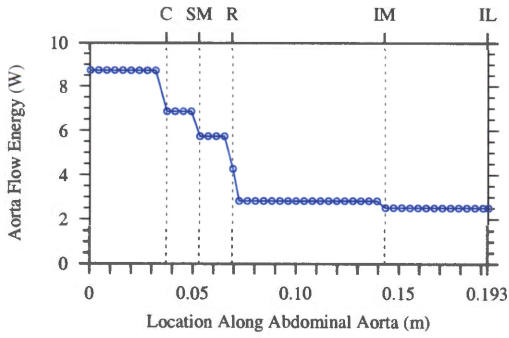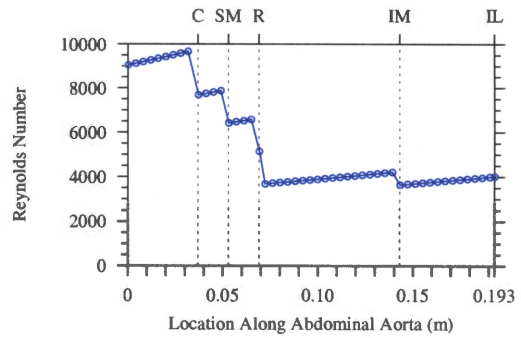(a) Physiological Diameter
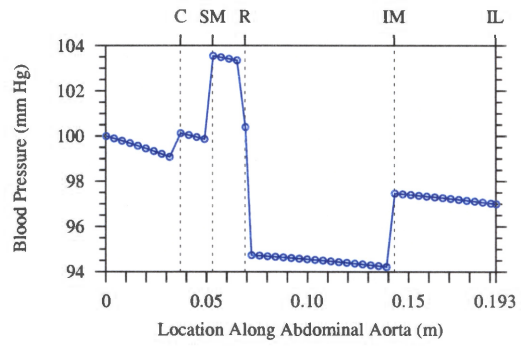
(b) Blood Pressure

(c) Velocity of Blood

(d) Wall Shear Stress

(e) Aorta Flow Energy

(f) Reynolds Number

Figure 3.7: *Results for Model of Tapered Elastic Vessel with Branches.*

42

branch flow exiting the main aorta artery. The wall shear stress, as seen in **Figure 3.7(d)**, follows the same trend as velocity; increasing and decreasing at the same locations along the length of the abdominal aorta. It can be seen that the minimum velocity and wall shear stress take place at the infrarenal section of the aorta as opposed to the suprarenal location. Previous studies, such as those mentioned in Chapter 1, have also found that wall shear stress and velocity tend to decrease after the right and left renal arteries (before the bifurcation into the right and left iliacs). It has also been observed that these locations are where atherosclerotic plaques are most likely to occur. This low wall shear stress and velocity environment at the infrarenal location is conducive to the formation of plaque since the low velocity allows the thrombi to organize and increase the plaque thickness, resulting in the decrease of the arterial lumen size. Therefore, blood flow through the artery is obstructed.

The change in pressure at the branch locations is given by the following equation

$$
\left(\frac{\dot{m}_{in} P_{in} - \dot{m}_{out} P_{out}}{\rho g} \right) = -\left(\frac{\dot{m}_{in} V_{in}^2 - \dot{m}_{out} V_{out}^2}{2g} \right) - \left(\dot{m}_{in} z_{in} - \dot{m}_{out} z_{out} \right)
$$
$$
+ \int_{x_{in}}^{x_{out}} \left(\frac{V_B^2}{2g} + z_B + \frac{P_B}{\rho g} \right) d\dot{m}_B + \int_{x_{in}}^{x_{out}} \frac{fV^2 (\rho V A)}{2gD} dx.
$$

$$(3.8)$$

The decrease in velocity that occurs at the branch locations tends to increase the pressure, but depletion of energy resulting from the branch flows exiting the abdominal aorta (and friction) causes the pressure to decrease. When the effect of velocity decrease is greater than the effect of energy depletion, the pressure increases. As seen in **Figure 3.7(b)**, this occurs at the celiac, superior mesenteric, and the inferior mesenteric arteries. When the effect of energy depletion is greater than the effect of velocity decrease, the pressure decreases. As shown in **Figure 3.7(b)**, this occurs at the left and right renal arteries. Between the branch locations the pressure decreases as the velocity increases according to the energy equation.

The Reynolds number was also plotted and can be seen in **Figure 3.7(f)**. As a result

of the velocity decrease at each of the branches, the Reynolds number also decreases. It can also be seen that, between the branches, Reynolds number stays constant since the effect of increasing velocity is offset by the effect of decreasing diameter. In this study the values for Reynolds number were found to stay above 2300; therefore, the flow through the abdominal aorta was found to be turbulent. Values for the average Reynolds number given in literature range from 550 to 1150 for the abdominal aorta (Moore 1991). The reason for this discrepancy is a subject for future study; however, possible sources for the discrepancy are that the current study does not account for pulsatile blood flow and uses a constant coefficient of viscosity.

Chapter 4

Conclusions and Recommendations

4.1 Conclusions

The results from this study show the importance of including both taper and elasticity in a model of the abdominal aorta. The taper of the abdominal aorta was found to have a significant effect on the magnitude of the velocity and the velocity profile along the length of the abdominal aorta. As seen in **Figures 3.3** and **3.6**, including taper in the model results in a lower velocity which increases along the length of the abdominal aorta as the diameter decreases. Including elasticity in the model allows the aortic walls to stretch and expand. The resulting change in diameter of the abdominal aorta has a significant effect on the blood flow velocity. For the straight model, the velocity increases when elasticity is included. However, for the tapered model, the velocity decreases when elasticity is included. Therefore, when looking at the effects of branch flows, only the elastic tapered model was used.

The model that included branch flows produced results that correlated well with previous studies with the exception of Reynolds number which was found to be much higher than in previous studies. The blood flow velocity through the abdominal aorta was found

45

to decrease at each location where the branch flows exit. The minimum velocity and wall shear stress were found to occur at the infrarenal section of the abdominal aorta. This finding is significant since previous studies have shown that this particular location along the abdominal aorta is prone to atherosclerotic plaque formation due to the low velocity and low wall shear stress that are found here under conditions of rest.

While it is clear that it is important to include elasticity, taper, and branch flows when modeling blood flow through the aorta, the branch flows have the greatest effect on the blood flow. Without the branch flows the models did not accurately predict the location of minimum velocity and wall shear stress at the infrarenal location where atherosclerotic plaque is more prone to develop. Taper is secondary in importance. Models without taper did not accurately predict the profile of the hemodynamic factors over the length of the abdominal aorta. Including elasticity in the model tends to refine the determination of the hemodynamic factors, but does not change their behavioral trends.

4.2   Recommendations for Future Work

Throughout this study the models were run for a case in which a human was lying down; therefore, the effects of potential energy on the blood flow were neglected. In future studies, models should also be ran that account for the effects of the potential energy of the blood flow when a human is in the upright position. Future studies should determine the importance of accounting for the pulsatile nature of the blood flow. The model can also be used to simulate the effects that atherosclerotic plaque would have on the blood flow through the aorta.

Bibliography

Bibliography

anon. (1981). Arteriosclerosis. Technical Report NIH Publication No. 81-2304, Report of the Working Group on Arteriosclerosis of the National Heart, Lung and Blood Institute.

Bergel, D. H. (1961). The static elastic properties of the arterial wall. *Journal of Physiology 156*, 445–457.

Caro, C. G., T. J. Pedley, R. C. Schroter, and W. A. Seed (1978). *The Mechanics of the Circulation*. Oxford University Press.

Cornhill, J. F., E. E. Herderick, and H. H. Stary (1990). Topography of human aortic sudanophilic lesions. D. W. Liepsch (Ed.), *Blood Flow in Large Arteries: Applications to Atherogenesis and Clinical Medicine*, pp. 13–19. Karger, Basel.

Cybulsky, M. I. and M. A. Gimbrone (1991). Endothelial expression of a mononuclear leukocyte adhesion molecule during atherogenesis. *Science 251*, 788–791.

Fox, J. A. and A. E. Hugh (1966). Localization of atheroma: A theory based on boundary-layer separation. *British Heart Journal 26*, 388–399.

Fung, Y. C. (1997). *Biomechanics: Circulation* (2nd ed.). Springer-Verlag.

Geneser, F. (1986). *Textbook of Histology*. Munksgaard.

Glagov, S., C. K. Zarins, D. P. Giddens, and D. N. Ku (1988). Hemodynamics and atherosclerosis, insights and perspectives gained from studies of human arteries. *Archives of Pathology and Laboratory Medicine 112*, 1018–1031.

Koehler, K. R. (1996). Blood velocity and turbulence. Electronic hypertext document, `www.physics.uq.edu.au/ph128/3e.html`. The University of Queensland, Australia.

Ku, D. N. (1997). Blood flow in arteries. *Annual Review of Fluid Mechanics 29*, 399–434.

Lee, D. and J. Y. Chen (2002). Numerical simulation of steady flow fields in a model of abdominal aorta with its peripheral branches. *Journal of Biomechanics 35*, 1115–1122.

Lelkes, P. I. (Ed.) (1999). *Mechanical Forces and the Endothelium*. Harwood Academic Publishers.

Liepsch, D. W. (1986). Flow in tubes and arteries – a comparison. *Biorheology 23*, 395–433.

McDonald, D. A. (1974). *Blood Flow in Arteries* (2nd ed.). The Williams & Wilkins Company.

Moore, J. E. (1991). *Magnetic Resonance Imaging Measurements of Pulsatile Hemodynamics in a Model of the Human Abdominal Aorta*. Ph. D. dissertation, Georgia Institute of Technology.

Moore, J. E. and D. N. Ku (1994a, August). Pulsatile velocity measurements in a model of the human abdomial aorta under resting conditions. *Journal of Biomechanical Engineering 116*, 337–346.

Moore, J. E. and D. N. Ku (1994b, February). Pulsatile velocity measurements in a model of the human abdomial aorta under simulated exercise and postprandial conditions. *Journal of Biomechanical Engineering 116*, 107–111.

Nerem, R. M. and W. A. Seed (1972). An *in vivo* study of aortic flow disturbances. *Cardiovascular Research 6*, 1–14.

Nobutaka, I., S. Ramasamy, T. Fukai, R. Nerem, and D. G. Harrison (1996). Shear stress modulates expression of cu/zn superoxide dismutase in human aortic endothelial cells. *Circulation Research 79*, 32–37.

Noria, S., F. Xu, S. McCue, M. Jones, A. I. Gotlieb, and B. L. Langille (2004, April). Assembly and reorientation of stress fibers drives morphological changes to endothelial cells exposed to shear stress. *American Journal of Pathology 164*(4), 1211–1223.

Patel, D. J. and R. N. Vaishnav (1980). *Hemodynamics and Its Role in Disease Processes*. University Park Press.

Pedersen, E. M., S. Oyre, M. Agerbæk, I. B. Kristensen, S. Ringgaard, P. Boesiger, and W. P. Paaske (1999). Distribution of early atherosclerotic lesions in the human abdominal aorta correlates with wall shear stresses measured *In Vivo*. *European Journal of Vascular and Endovascular Surgery 18*, 328–333.

Pedersen, E. M., H.-W. Sung, A. C. Burlson, and A. P. Yoganathan (1993). Two-dimensional velocity measurements in a pulsatile flow model of the normal abdominal aorta simulating different hemodynamic conditions. *Journal of Biomechanics 26*(10), 1237–1247.

Porenta, G., D. F. Young, and T. R. Rogge (1986, May). A finite-element model of blood flow in arteries including taper, branches, and obstructions. *Journal of Biomechanical Engineering 108*, 161–167.

Ross, J. (1999). Structure and function of blood vessels. Electronic hypertext document, `greenfield.fortunecity.com/rattler/46/vessels.htm`. University of Luton, United Kingdom.

Sapirstein, L. A. (1958). Regional blood flow by fractional distribution indicators. *Journal of Applied Physiology 193*, 161–168.

Sessa, W., K. Pritchard, N. Seydi, J. Wang, and T. Hintze (1994). Chronic exercise in dogs increases coronary vascular nitric oxide production in endothelial cell nitric oxide synthase gene expression. *Circulation Research 74*, 349–353.

Spence, A. P. and E. B. Mason (1987). *Human Anatomy and Physiology* (3rd ed.). The Benjamin/Cummings Publishing Company, Inc.

Strong, J. P., G. T. Malcom, C. A. McMahan, R. E. Tracy, W. P. Newman, E. E. Herderick, and J. F. Cornhill (1999). Prevalence and extent of atherosclerosis in adolescents and young adults: Implication for prevention from pathobiological determinants of atherosclerosis in youth study. *Journal of the American Medical Association 281*, 727–735.

Taylor, C. A., C. P. Cheng, L. A. Espinosa, B. T. Tang, D. Parker, and R. J. Herfkens (2002). *In Vivo* quantification of blood flow and wall shear stress in the human abdominal aorta during lower limb exercise. *Annals of Biomedical Engineering 30*, 402–408.

Thibodeau, G. A. and K. T. Patton (1996). *Anatomy and Physiology* (3rd ed.). Mosby-Year Book, Inc.

Wang, J., S. M. Wolin, and H. T. Hintze (1993). Chronic exercise enhances endothelium-mediated dilation of epicardial coronary artery in conscious dogs. *Circulation Research 73*, 829–838.

White, F. M. (1986). *Fluid Mechanics* (2nd ed.). McGraw-Hill, Inc.

Wilson, S. E., F. J. Veith, R. W. Hobson, and R. A. Williams (1987). *Vascular Surgery Principals and Practice*. McGraw-Hill, Inc.

Zarins, C. K., R. A. Bomberger, and S. Glagov (1981). Local effects of stenoses: Increased flow velocity inhibits atherogenesis. *Circulation 64*, II–221–227.

Appendix

Appendix A

Derivation of Equation 2.5

For any fluid property, B, the amount of B contained within a control volume is given by

$$B = \int_{CV} \rho b \, dV \tag{A.1}$$

where ρ is the fluid density and b is the intensive value of B. The rate of change of B within the control volume is given by Reynolds Transport Theorem

$$\frac{DB}{Dt} = \iiint_{CV} \frac{\partial}{\partial t}(\rho b) \, dV + \iint_{CS} \rho b \, \vec{v} \cdot \hat{n} \, dA \tag{A.2}$$

where the first term on the right-hand side of the equation represents the change in B stored within the control volume and the second term represents the net flux of B entering and leaving through the control surface. Using Gauss' Theorem, the flux term can be rewritten as

$$\iint_{CS} \rho b \, \vec{v} \cdot \hat{n} \, dS = \iiint_{CV} \mathrm{div}(\rho b \vec{v}) \, dV \tag{A.3}$$

or

$$\iint_{CS} \rho b \, \vec{v} \cdot \hat{n} \, dS = \iiint_{CV} \left(\frac{\partial}{\partial x}(\rho b v_x) + \frac{\partial}{\partial y}(\rho b v_y) + \frac{\partial}{\partial z}(\rho b v_z) \right) dV. \tag{A.4}$$

Applied to one-dimensional flow through a pipe (or artery) with an exiting branch flow,

$$B = \int_{CV} \rho b \, dV = \int_{CV_1} \rho b \, dV_1 + \int_{CV_2} \rho b \, dV_2 \tag{A.5}$$

where CV_1 is a control volume within the main flow path (the abdominal aorta) and CV_2 is a control volume within the branch flow exiting CV_1. Taking into account the geometry of the main flow path, Equation A.5 becomes

$$B = \int_{x_1}^{x_2} \rho b A \, dx + \int_{CV_2} \rho b \, dV_2. \tag{A.6}$$

55

Thus, the Reynolds Transport Theorem becomes

$$\frac{DB}{Dt} = \iiint\limits_{CV} \frac{\partial}{\partial t}(\rho b)\, dV + \iiint\limits_{CV} \text{div}(\rho b \vec{v})\, dV + \frac{D}{Dt}\int\limits_{CV_2} \rho b\, dV_2 \qquad (A.7)$$

or, taking into account the one-dimensional geometry of the main flow path,

$$\frac{DB}{Dt} = \int\limits_{x_1}^{x_2} \frac{\partial}{\partial t}(\rho b A)\, dx + \int\limits_{x_1}^{x_2} \frac{\partial}{\partial t}(\rho b A v_x)\, dx + \frac{D}{Dt}\int\limits_{CV_2} \rho b\, dV_2. \qquad (A.8)$$

Letting $B = m$ (and thus $b = 1$) to obtain an expression for the conservation of mass yields

$$\frac{DB}{Dt} = \int\limits_{x_1}^{x_2} \frac{\partial}{\partial t}(\rho A)\, dx + \int\limits_{x_1}^{x_2} \frac{\partial}{\partial t}(\rho A v_x)\, dx + \frac{D}{Dt}\int\limits_{CV_2} \rho\, dV_2 = 0. \qquad (A.9)$$

For an incompressible substance ($\rho =$ constant)

$$\frac{DB}{Dt} = \int\limits_{x_1}^{x_2} \left(\frac{\partial}{\partial t}(A) + \frac{\partial}{\partial t}(A v_x) \right) dx + \frac{1}{\rho}\frac{D}{Dt}\int\limits_{CV_2} \rho\, dV_2 = 0. \qquad (A.10)$$

But,

$$\frac{1}{\rho}\frac{D}{Dt}\int\limits_{CV_2} \rho\, dV_2 = \int\limits_{x_1}^{x_2} q\, dx. \qquad (A.11)$$

Substituting this back into Equation A.10 yields

$$\int\limits_{x_1}^{x_2} \left(\frac{\partial A}{\partial t} + \frac{\partial}{\partial t}(A v_x) + q \right) dx = 0; \qquad (A.12)$$

therefore,

$$\frac{\partial A}{\partial t} + \frac{\partial A v_x}{\partial t} + q = 0. \qquad (A.13)$$

56

Appendix B

Calculation of Taper Factor for the Abdominal Aorta

According to Fung (1997), the change in the area of the aorta due to tapering, fits the exponential equation,

$$A(x) = A_{in} e^{-Bx/r_{in}} \qquad \text{(B.1)}$$

where r_{in} is the inlet radius of abdominal aorta. Defining the taper factor as $k = B/r_{in}$, the equation becomes

$$A(x) = A_{in} e^{-kx}. \qquad \text{(B.2)}$$

Therefore, at the exit of the abdominal aorta,

$$A(x = x_{out}) = A_{in} e^{-kx_{out}} \qquad \text{(B.3)}$$

or

$$\frac{A_{out}}{A_{in}} = e^{-kx_{out}}. \qquad \text{(B.4)}$$

Taking the natural logarithm of both sides yields

$$\ln\left(\frac{A_{out}}{A_{in}}\right) = -kx_{out} \qquad \text{(B.5)}$$

or, solving for the taper factor, k,

$$k = -\frac{1}{x_{out}} \ln\left(\frac{A_{out}}{A_{in}}\right). \qquad \text{(B.6)}$$

Finally, substituting for the cross-sectional areas using $A = \pi D^2/4$ yields

$$k = -\frac{1}{x_{out}} \ln\left(\frac{D_{out}^2}{D_{in}^2}\right). \qquad \text{(B.7)}$$

Using values cited by Moore and Ku (1994a) for the inlet and outlet diameters of the abdominal aorta of $D_{in} = 0.025$ m and $D_{out} = 0.018$ m at $x_{out} = 0.193$ m, Equation B.7 yields a value for taper factor of $k = 3.40$ 1/m.

Vita

Amber Adriann Hensley Edwards was born in Knoxville, TN, on October 12, 1978. She attended Jefferson Junior High School and graduated from Oak Ridge High School in May 1996. She attended East Tennessee State University the following fall where she studied pre-medicine. However, with her love for both science and mathematics, she decided to pursue a career in engineering and enrolled in the University of Tennessee, Knoxville, in Spring 1998. She received the degree of Bachelor of Science in Engineering Science with a concentration in Biomedical Engineering in May 2001. She continued her education at UTK earning the degree of Master of Science in Mechanical Engineering in August 2004.